

## Supporting Information

### **Plasmonic Gold Nanocrystals Stimulated Efficiently Photocatalytic Nitrogen Fixation over Mo Doped $W_{18}O_{49}$ nanowires**

Peng Qiu,<sup>a</sup> Cong Huang,<sup>a</sup> Gang Dong,<sup>a</sup> Feiyang Chen,<sup>a</sup> Feifan Zhao,<sup>a</sup> Yongsheng Yu,<sup>[b]</sup> Xueqin Liu,<sup>a</sup> Zhen Li<sup>a</sup> and Yang Wang<sup>\*a</sup>

*a. Faculty of Materials Science and Chemistry, China University of Geosciences, Wuhan 430074, PR China.*

*b. College of Chemistry and Chemical Engineering, Xinyang Normal University, Xinyang, Henan 464000, P. R. China.*

*\* Corresponding author: wyisian@cug.edu.cn (Yang Wang).*

### ***Turnover number (TON) calculation.***

Turnover number (TON) is usually defined by the number of reacted molecules to that of an active site (Eq (1)).<sup>1-5</sup>

$$TON = \frac{\text{Number of reacted molecules}}{\text{Number of active sites}} \quad (1)$$

However, it is difficult to determine the exact number of active sites on the solid catalyst. So, we define the number of reacted electrons to the number of Mo atoms as the TON (2) of the photocatalyst.

$$TON = \frac{\text{Number of reacted electrons}}{\text{Number of Mo atoms in photocatalyst}} = \frac{3n(NH_3)}{n(Mo)} \quad (2)$$

It is worth noting that the active sites of Mo-W on the surface is relatively few that TON (2) is smaller than the real TON (1).

The photocatalytic N<sub>2</sub> reduction reaction (NRR) performance of the photocatalysts was evaluated in a photocatalytic reactor with a quartz glass window under atmospheric pressure and ambient temperature. 20 mg Au-MWO catalyst was added into 100 mL methanol aqueous solution, and the corresponding NH<sub>3</sub> production yield was 1.437 mg/L. The n(NH<sub>3</sub>) was calculated to be 7.9848 × 10<sup>-6</sup> mol. The total amount of Mo was 1.63 × 10<sup>-6</sup> mol. The TON was calculated to be (3 × 7.9848 × 10<sup>-6</sup>) / 1.63 × 10<sup>-6</sup> = 14.70.

## Figures and Table.

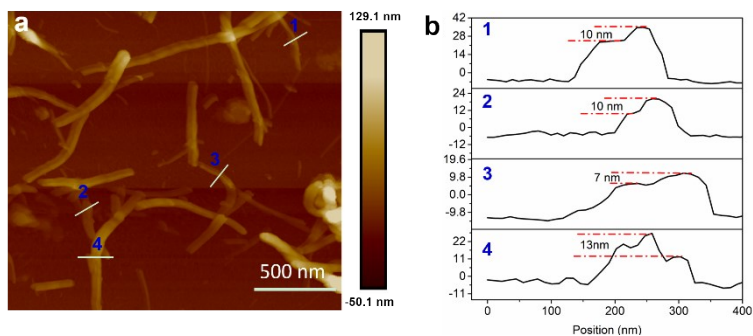


**Figure S1.** AFM analysis of the Au-MWO nanowires: (a) AFM image of the nanowires, (b) height profiles along the white lines in (a).

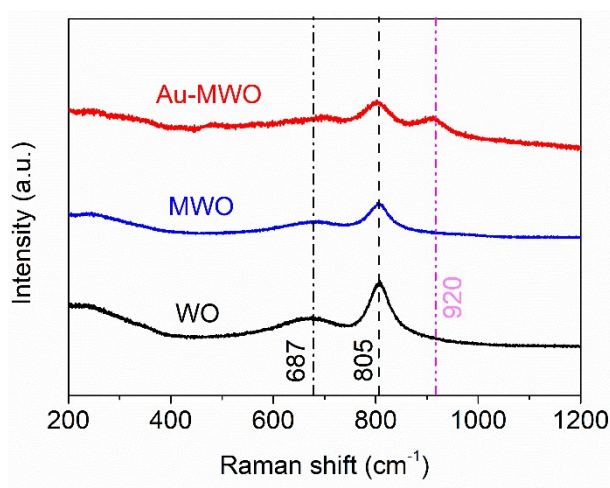


**Figure S2.** Raman spectra of WO, MWO and Au-MWO.

Raman spectra of WO and MWO shows two intense Raman peaks at 805  $\text{cm}^{-1}$  and 687  $\text{cm}^{-1}$ , which can be assigned to the symmetric and asymmetric stretching vibrations of  $\text{W}^{6+}\text{-O}$  bond, respectively. As can be seen from Au-MWO spectrum, an obvious band representing Au nanoparticles appears at the location 920  $\text{cm}^{-1}$ , which also indicates the successful introduction of Au nanoparticles.<sup>6</sup>

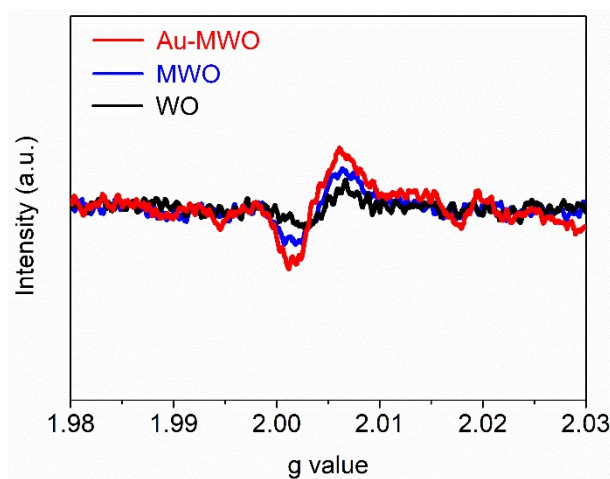


**Figure S3.** EPR spectra of WO, MWO and Au-MWO samples at room temperature.

The three samples of WO, MWO and Au-MWO all exhibit a pair of sharp symmetric peaks in accordance with the oxygen vacancy signal at  $g = 2.003$ , which indicates electron trapping at oxygen vacancies. Moreover, all of three samples show an indistinguishable strength of the peak. It indicated that Mo doping and Au deposition did not introduce extra oxygen vacancies. This is consistency with the result of the O 1s XPS (**Figure 2f**) and the calculated slab energies of various Mo-doped models.

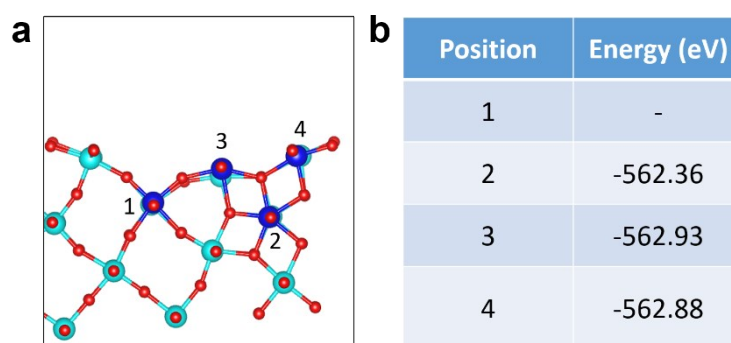


**Figure S4.** Possible sites of Mo doping to replace W atom in WO model.

In order to determine the location of doped Mo atoms, we calculate the energies of Mo doped WO with different doping configurations, as illustrated in **Figure S4a**. The slab energies of Mo doped models are summarized in **Figure S4b**. Position 3 with Mo–W bond exhibits the lowest energy among all configurations, which has been applied in our calculations.

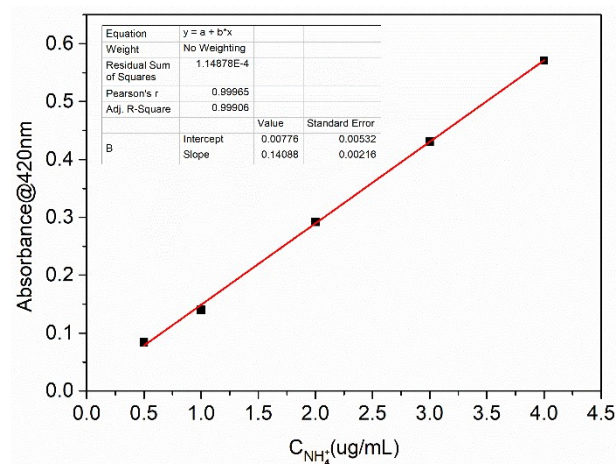


**Figure S5.**  $\text{NH}_4^+$  quantification using Nessler's reagent.

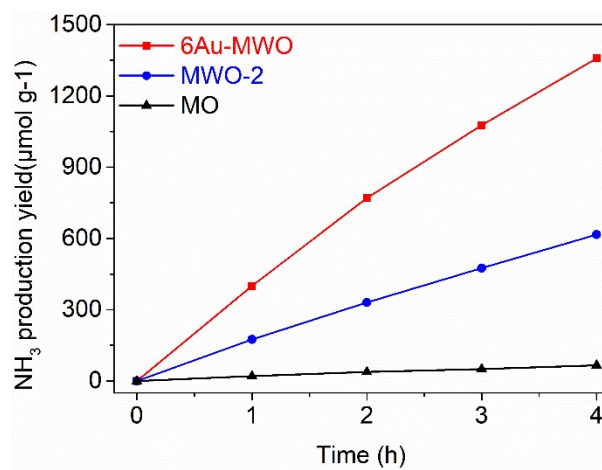


**Figure S6.** Time-dependent  $\text{NH}_3$  yield for WO, MWO-2 and 6Au-MWO.

The photocatalytic nitrogen fixation rates of photocatalysts still maintain high stability with continuous irradiation for 4 h, as shown in **Figure S6**. It also demonstrated the high photostability of photocatalysts.

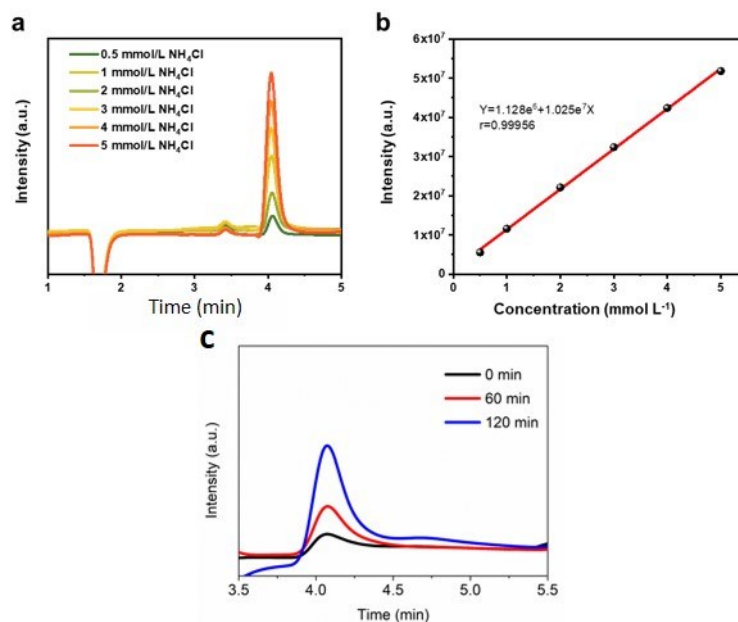


**Figure S7.** (a, b) Standard curve of  $\text{NH}_4^+$  with ion chromatography. (c) The ammonium ion chromatograms of 6Au-MWO under different time.

The ion chromatography had been performed to detect the produced ammonia accurately. Standard curve of  $\text{NH}_4^+$  with ion chromatography was drawn under the condition of methane sulfonic acid as eluent, as shown in **Figure S7a** and **S7b**. The ammonia yield of 6Au-MWO under different time was detected to verify the accuracy of nitrogen fixation rate. As shown in **Figure S7c**, the comparable nitrogen fixation rate ( $389.01 \mu\text{mol g}^{-1} \text{h}^{-1}$ ) verified the accuracy of produced ammonia.

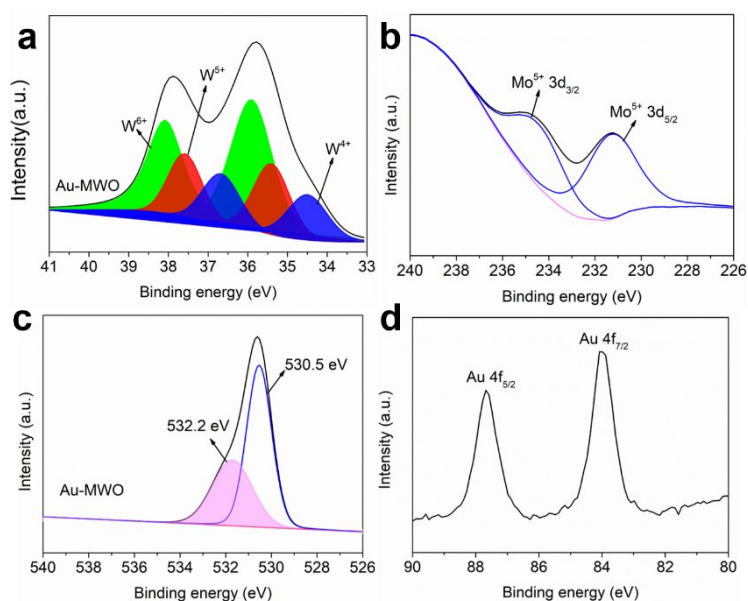


**Figure S8.** The (a) W 4f, (b) Mo 3d, (c) O 1s and (d) Au 4f XPS spectra of Au-MWO after cyclic tests.

The characterization of chemical states before and after photocatalytic reaction is an important way to evaluate the stability of photocatalyst. The chemical states of the Au-MWO after the stability tests were characterized by XPS. As shown in **Figure S8**, the unaltered chemical states of Mo and O indicated the high stability of the photocatalyst.

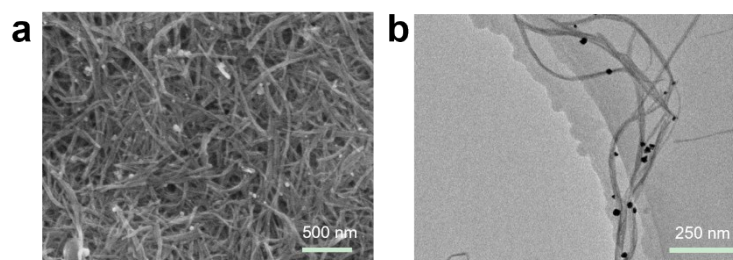


**Figure S9.** (a) SEM and (b) TEM images of 6Au-MWO after cyclic tests.

The SEM and TEM measurements of 6Au-MWO after the stability tests had been conducted. As shown in **Figure S9**, the 6Au-MWO still keeps the unchanged morphology of nanowire. This demonstrates the excellent reusability and stability of 6Au-MWO for photocatalytic  $N_2$  fixation.

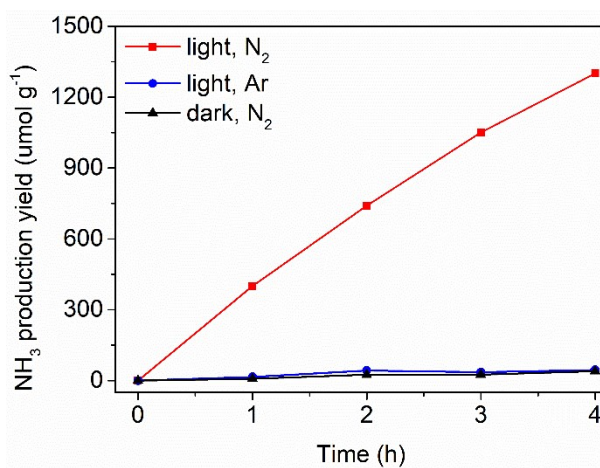


**Figure S10.** Photocatalytic nitrogen fixation over 6Au-MWO under different conditions ( $N_2$  and Ar with irradiation,  $N_2$  without irradiation).

As compared to the considerable nitrogen fixation capacity of 6Au-MWO in  $N_2$ -saturated water with irradiation, ignorable  $NH_3$  yield was observed in Ar-saturated water with irradiation and  $N_2$ -saturated water without irradiation, indicating that  $N_2$  is the only source of  $NH_3$  obtained by photocatalytic nitrogen fixation process.

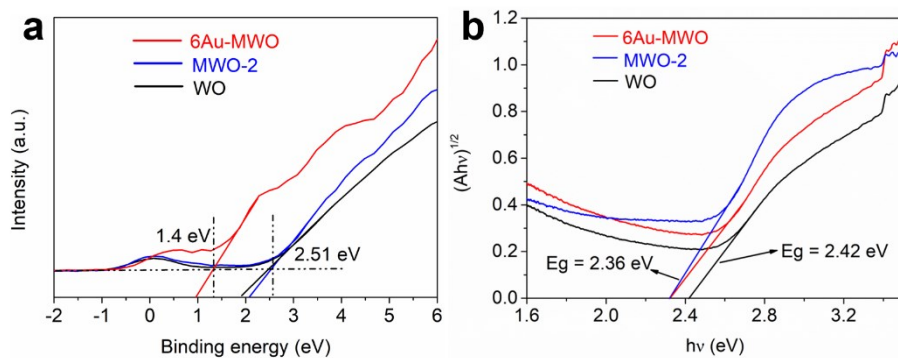


**Figure S11.** (a) Valence-band XPS spectra of WO, MWO-2 and 6Au-MWO. (b) Tauc plots of the three catalysts. The curves were converted from the absorption spectra shown in **Figure 4e**.

**Table S1.** Representative works on photocatalytic N<sub>2</sub> fixation.

Photocatalysts	Light source	Conditions	NH <sub>3</sub> yield rate	AQE	Ref.
Au-MWO	full spectrum	methanol	399 μmol g <sup>-1</sup> h <sup>-1</sup>	0.61% at 540 nm	This work
Pothole-rich WO <sub>3</sub>	full spectrum	water	NO <sub>3</sub> <sup>-</sup> : 1.92 mg g <sup>-1</sup> h <sup>-1</sup>	0.11% at 380 nm	7
C-WO <sub>3</sub> ·H <sub>2</sub> O	visible light	water	63.55 μmol g <sup>-1</sup> h <sup>-1</sup>	--	8
W <sub>18</sub> O <sub>49</sub>	full spectrum	water	65.2 μmolL <sup>-1</sup> g <sup>-1</sup> h <sup>-1</sup>	9% at 365 nm	9
TiO <sub>2</sub> /Au/a-TiO <sub>2</sub>	AM1.5G	water	13.4 nmol cm <sup>-2</sup> h <sup>-1</sup>	--	10
Bi <sub>5</sub> O <sub>7</sub> Br-OV	λ > 420 nm	water	1.38 mmol g <sup>-1</sup> h <sup>-1</sup>	--	11
BiOBr-OV	λ > 420 nm	water	104.2 μmol g <sup>-1</sup> h <sup>-1</sup>	0.23% at 420nm	12
Au/TiO <sub>2</sub> -OV	λ > 420 nm	methanol	130.5 μmol g <sup>-1</sup> h <sup>-1</sup>	0.82% at 550 nm	13
CuCr	λ > 420 nm	water	73.9 μmol g <sup>-1</sup> h <sup>-1</sup>	0.1% at 500 nm	14
TiO <sub>2</sub> -OV	λ > 280 nm	water	0.73 μmol g <sup>-1</sup> h <sup>-1</sup>	0.70% at λ < 350 nm	15
Mn-WO <sub>3</sub>	full spectrum	water	425 μmolL <sup>-1</sup> g <sup>-1</sup> h <sup>-1</sup>	0.18% at 450 nm	16
F-V <sub>0</sub> -TiO <sub>2</sub>	full spectrum	water	206 μmolL <sup>-1</sup> g <sup>-1</sup> h <sup>-1</sup>	0.38% at 420 nm	17

## References

1. J. Tian, Y. Zhang, L. Du, Y. He, X. Jin, S. Pearce, R. L. Harniman, D. Alibhai, R. Ye, D. L. Phillips and I. Manners, *Nat. Chem.*, 2020, **12**, 1150-1156.
2. A. Kudo and Y. Miseki, *Chem. Soc. Rev.*, 2009, **38**, 253-278.
3. D. Xu, B. Cheng, J. Zhang, W. Wang, J. Yu, and W. Ho, *J. Mater. Chem. A*, 2015, **3**, 20153-20166.
4. R. Hailili, C. Wang, E. Lichtfouse, *Appl. Catal. B*, 2018, **232**, 531-543.
5. Y. Zhang and T. Ren, *Chem. Commun.*, 2012, **48**, 11005-11007.
6. R. J. Bose, V.S. Kavitha, C. Sudarsanakumar, V.P. M. Pillai, *Appl. Surf. Sci.*, 2016, **379**, 505-515.
7. Y. Liu, M. Cheng, Z. He, B. Gu, C. Xiao, T. Zhou, Z. Guo, J. Liu, H. He, B. Ye, B. Pan, and Y. Xie, *Angew. Chem. Int. Ed.*, 2019, **58**, 731-735.
8. X. Li, W. Wang, D. Jiang, S. Sun, L. Zhang and X. Sun, *Chem. Eur. J.*, 2016, **22**, 13819-13822.
9. W. Ren, Z. Mei, S. Zheng, S. Li, Y. Zhu, J. Zheng, Y. Lin, H. Chen, M. Gu, and F. Pan, *Research*, 2020, **2020**, 3750314.
10. C. Li, T. Wang, Z. Zhao, W. Yang, J. Li, A. Li, Z. Yang, G. A. Ozin, and J. Gong, *Angew. Chem. Int. Ed.*, 2018, **57**, 5278-5282.
11. S. Wang, X. Hai, X. Ding, K. Chang, Y. Xiang, X. Meng, Z. Yang, H. Chen, and J. Ye, *Adv. Mater.*, 2017, **29**, 1701774.
12. H. Li, J. Shang, Z. Ai, and L. Zhang, *J. Am. Chem. Soc.*, 2015, **137**, 6393-6399.
13. J. Yang, Y. Guo, R. Jiang, F. Qin, H. Zhang, W. Lu, J. Wang, and J. C. Yu, *J. Am. Chem. Soc.*, 2018, **140**, 8497-8508.
14. Y. Zhao, Y. Zhao, G. I. N. Waterhouse, L. Zheng, X. Cao, F. Teng, L. Wu, C. Tung, D. O'Hare, and T. Zhang, *Adv. Mater.*, 2017, **29**, 1703828.
15. H. Hirakawa, M. Hashimoto, Y. Shiraishi, and T. Hirai, *J. Am. Chem. Soc.*, 2017, **139**, 10929-10936.
16. Y. Zhang, T. Hou, Q. Xu, Q. Wang, Y. Bai, S. Yang, D. Rao, L. Wu, H. Pan, J. Chen, G. Wang, J. Zhu, T. Yao, and X. Zheng, *Adv. Sci.*, 2021, **32**, 2100302.
17. R. Guan, D. Wang, Y. Zhang, C. Liu, W. Xu, J. Wang, Z. Zhao, M. Feng, Q. Shang, Z. Sun, *Appl. Catal. B*, 2021, **282**, 119580.